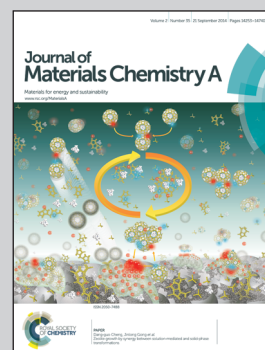**An article presented by Prof. Taiho Park, Chemical Engineering, POSTECH.**

Title: Doubly open-ended TiO$_2$ nanotube arrays decorated with a few nm-sized TiO$_2$ nanoparticles for highly efficient dye-sensitized solar cells

Simultaneously improved electron collection and light harvesting has been realized using a doubly open-ended TiO$_2$ nanotube array decorated with small-sized TiO$_2$ nanoparticles which shows improved power conversion efficiency compared to a conventional DSC employing TiO$_2$ nanoparticles.

As featured in:

ROYAL SOCIETY OF CHEMISTRY

www.rsc.org/MaterialsA

PAPER

Doubly open-ended TiO$_2$ nanotube arrays decorated with a few nm-sized TiO$_2$ nanoparticles for highly efficient dye-sensitized solar cells†

Jongmin Choi,‡ Young Soo Kwon‡ and Taiho Park*

Doubly open-ended TiO$_2$ nanotube (NT) arrays decorated with a few nm-sized TiO$_2$ nanoparticles (sNP@NT hybrid structure) were prepared and used as charge-collecting photoelectrodes in dye-sensitized solar cells (DSCs). The TiO$_2$ nanoparticles (NPs) on the NT array surfaces increased the dye loading on the sNP@NT-based DSCs by 9% compared to the undecorated NT-based DSCs, thereby enhancing the light harvesting capabilities. The power conversion efficiency (PCE) of the sNP@NT-based DSC prepared with 11 μm thick NT arrays was 10.0%, which constituted a 47% improvement over the corresponding NT-based DSCs (which displayed a 6.8% PCE). Despite having a dye loading level that was 22% lower than the dye loading level in the conventional TiO$_2$ NP-based DSCs, due to the limited internal surface area, the PCE of the sNP@NT-based DSC was 28% greater than that of the conventional TiO$_2$ NP-based DSC (8.1% PCE) prepared with a light scattering layer. The high charge collection efficiency of the NT array and the good photovoltaic performance set a new record for efficiency among NT-based DSCs.

1. Introduction

Dye-sensitized solar cells (DSCs) have been widely investigated in academia and industry as next-generation photocells. DSCs may be prepared through simple fabrication processes at low costs, and they provide high power conversion efficiencies (PCEs).[1] The photoanode of a typical DSC is prepared from a dye-coated optically transparent film composed of 20 nm TiO$_2$ nanoparticles (NPs) and a platinum counter-electrode arranged in a sandwich configuration.[2,3] The inter-electrode space is filled with a liquid electrolyte. Although the TiO$_2$ NPs provide a large internal surface area for anchoring large amounts of dye and maximizing the harvesting of incident light, photoinduced electrons generated in the NP film undergo random diffusive transport through the disordered film architecture. The charge collection properties of such films are poor. Recently, highly ordered TiO$_2$ nanotube (NT) arrays were examined as an alternative electron transport material because they can increase the electron collection through direct charge pathways;[4] however, the amount of dye that could be loaded into a NT-based film for light harvesting in a NT-based DSC was much lower than that in a NP-based DSC due to the lower surface area.[5]

Pohang University of Science and Technology, San 31, Nam-gu, Pohang, Kyoungbuk, Korea. E-mail: taihopark@postech.ac.kr; Fax: +82-54-279-8298; Tel: +82-54-279-2394

† Electronic supplementary information (ESI) available. See DOI: 10.1039/c4ta02360a

‡ These authors contributed equally to this work.

The PCE obtained from a DSC can be estimated through the equation:[6] PCE $= (J_{SC} \times V_{OC} \times FF)/P_{in}$, where J_{SC} is the short circuit current density (mA cm^{-2}), V_{OC} is the open circuit voltage, FF is the fill factor, and P_{in} is the input power. V_{OC} is primarily determined by the energy difference between the quasi-Fermi level of the nanocrystalline TiO$_2$ electrode under illumination and the redox potential of the I$_3^-$/I$^-$ couple. FF is governed by the electron transport properties through the electrolyte and the catalytic properties of the counter electrode.[7] Therefore, a higher J_{SC} could yield a better PCE for a given crystalline TiO$_2$ electrode, liquid electrolyte, and Pt counter electrode. The J_{SC} value is typically estimated from the equation:[4] $J_{SC} = q \times \eta_{lh} \times \eta_{inj} \times \eta_{cc} \times I_o$, where q is the fundamental charge of an electron, I_o is the intensity of the incident light, η_{lh} is the light harvesting efficiency, η_{inj} is the electron injection efficiency from an excited dye molecule into the TiO$_2$ conduction band, and η_{cc} is the charge collection efficiency of the injected electrons. We demonstrated that the NT-based DSC yielded an η_{cc} exceeding 95%, 15% greater than that observed for the NP-based DSC.[8] Assuming that the η_{inj} values were similar in both DSCs, the J_{SC} value in the NT-based DSC could be improved by increasing the η_{lh} value. This may be achieved by increasing the dye loading value on the larger photoanode surface area.

The use of thicker NTs could be a way to increase the dye loading, but injected electrons have a longer pathway in thicker NTs, undergoing numerous charge recombination events with oxidized species in electrolytes.[9] This is resulted in the decreased J_{SC} as well as V_{OC}.[9,10] Alternatively, modifications of

14380 | J. Mater. Chem. A, 2014, 2, 14380–14385

This journal is © The Royal Society of Chemistry 2014

the NT surface such as controlling the morphology of the NTs,[11,12] altering NT walls,[13–15] or fabricating NT/NP hybrid structures[16,17] have been widely investigated. These methods are useful for increasing the NT surface area;[18] however, controlling the NT morphology by, for example, decreasing the tube diameter usually shortens the tube length.[11,12] Alteration of NT walls, such as introducing double walls[13] or creating bamboo-type NTs,[14,15] requires complex fabrication processes and provides low PCE (2.96%). NT/NP hybrid structures, in which the NT walls are decorated with small NPs, may be readily obtained from Ti(OH)$_4$ prepared from TiCl$_4$ in water.[4,14] Most NT/NP hybrid photoanodes are based on singly opened NT arrays that include a barrier layer in the bottom region of the NT arrays.[17,19–21] The barrier layer can disrupt the flow of electrolytes to the inside of the tube and can reflect the near-UV light.[22] The barrier, therefore, reduces the efficiencies of NT-based DSCs and yields relatively low PCEs of 3.8–7.56%. We recently reported a method for selectively etching the aligned doubly open-ended TiO$_2$ nanotubes. The amorphous doubly open-ended TNTs were easily transferred to an FTO substrate to fabricate front-illuminated DSCs.[8] We demonstrated that the NT-based DSC provided a better PCE than the NP-based DSC mainly by improving the efficiency of η_{cc}, which increased V_{OC}, despite a dye loading in the NT-based DSCs that was 20% lower than in the NP-based DSCs. The decoration of the small TiO$_2$ NPs on the aligned doubly open-ended TiO$_2$ NTs (denoted sNP@NTs) may increase the dye loading on the photoanode and improve J_{SC} by increasing η_{lh}. Here, we report the development of a highly efficient DSC prepared using sNP@NTs consisting of doubly open-ended TiO$_2$ NT arrays decorated with NPs a few nm in size. The sNP@NT-based DSCs prepared with NT arrays only 11 μm thick exhibited a PCE exceeding 10.0%, higher than the PCEs obtained from conventional DSCs prepared with scattering layers (a 21 μm thick DSC yielded a PCE of 8.1%).

2. Experimental section

2.1 Preparation of freestanding doubly open-ended TiO$_2$ NTs

All anodization experiments were carried out in ethylene glycol solution containing 0.25 wt% NH$_4$F and 0.3 vol% distilled water at room temperature. TiO$_2$ NT arrays were prepared by anodization of Ti foil (99.7%, 0.25 mm, Aldrich) in a two electrode electrochemical cell with carbon sheets as the counter electrode. Before anodization, Ti foil was ultrasonically washed with acetone, ethanol, and distilled water. The anodization process was divided into two steps. At the first step, the Ti foil was anodized at 60 V for 120 min, and the resulting sample was ultrasonically washed with ethanol to remove the electrolyte and debris, followed by annealing at 250 °C for 2 h. The annealed sample was anodized again under the same anodizing conditions for a short time (5–10 min). After these two steps, the anodized sample was immersed in 33 wt% H$_2$O$_2$ solution. After ca. 5 min, the NT arrays with a closed bottom were separated from the Ti foil, and the closed bottom layer of TiO$_2$ NT arrays became opened with increase immersing time. After the etching

process, doubly open-ended TiO$_2$ NT arrays were washed with ethanol and dried in air.

2.2 Fabrication of DSCs

The as-prepared TiO$_2$ NT membrane was adhered onto the fluorine doped Tin oxide (FTO) glass substrate using viscous TiO$_2$ nanoparticle (NP) paste, which was printed onto FTO glass by the doctor-blade technique. The fixed TiO$_2$ NT on the NP film was annealed at 550 °C for 30 min, followed by immersion in 0.03 mM (Bu4N)$_2$Ru(dcbpyH)$_2$-(NCS)$_2$ (N719 dye) solution for 24 h. The TiO$_2$ electrode was rinsed with acetonitrile in order to remove physically adsorbed dyes. The dye-absorbed TiO$_2$ electrodes were sandwiched together with a Pt-coated FTO glass counter electrode using a 60 μm thick-hot-melt spacer. The electrolyte, 0.03 M I$_2$, 0.6 M 1-butyl-3-methylimidazolium iodide (BMII), 0.1 M guanidinium thiocyanate, 0.5 M LiI, and 0.5 M 4-tert-butylpyridine (tBP) in acetonitrile and valeronitrile (85 : 15 v/v%), was introduced into the space between the sandwiched cells.

2.3 Characterization

2.3.1 X-ray diffraction measurement. X-ray diffraction analysis (XRD, Rigaku D/Max-2200/PC) was employed for crystal phase identification. The angle range examined was 20–80 degree at the theta–2theta scan mode.

2.3.2 Scanning electron microscopy (SEM) measurement. A field emission scanning electron microscope (FE-SEM, Hitachi S 4800) was utilized for morphological and structural characterization.

2.3.3 Photoelectrochemical measurement. The current–voltage characteristics were measured using a Keithley 2400 source meter under simulated AM 1.5G illumination (100 mW cm^{-2}) provided by a solar simulator (69920, 1 kW Xe lamp with an optical filter, Oriel) to determine open-circuit voltage (V_{OC}), short-circuit current (J_{SC}), fill factor (FF), and conversion efficiency (η). The incident light intensity was calibrated with a Si solar cell (as a reference) equipped with an IR-cutoff filter (KG-5, Schott). The voltage step and delay time for the measurement were 10 mV and 40 ms, respectively.

2.3.4 UV-Vis absorption measurement. UV-Vis spectrophotometry (using an Optizen POP spectrophotometer) was used to measure the adsorbed dye amount onto the TiO films, and dye detached by immersing a 0.1 M KOH aqueous solution for 30 min, followed by measuring the absorbance of the resulting solution.

2.3.5 Electrochemical impedance spectrophotometry measurement. The impedance values of DSCs having different electrodes were measured using a computer-controlled potentiostat (SP-200, BioLogic) under dark conditions. The frequency range examined was 0.005 Hz to 100 kHz at room temperature, and the impedance spectra were recorded at potentials that varied from −0.66 to −0.72 V with a voltage amplitude set at 10 mV. The photo-injected electron life time was calculated from the middle frequency (f_{min}, $\tau_{rec} = 1/2\pi f_{min}$) of Nyquist spectra. The recorded spectra were fit to an appropriate

This journal is © The Royal Society of Chemistry 2014

J. Mater. Chem. A, 2014, **2**, 14380–14385 | **14381**

simplified circuit (Model S1) using the Z-fit software provided by BioLogic.

$$\text{Model S1}: R_s + \begin{bmatrix} R_1 \\ Q_1 \end{bmatrix} + \begin{bmatrix} R_2 \\ Q_2 \end{bmatrix}$$

2.3.6 The incident photon-to-current efficiency (IPCE) spectra measurements. The IPCE spectra were plotted as a function of wavelength under a constant white light bias of approximately 5 mW cm^{-2} supplied by an array of white light emitting diodes using a power source with a monochromator (Zahner GmbH) and a multimeter and chopped at approximately 5 Hz.

3. Results and discussion

Fig. 1 illustrates the process used to fabricate an sNP@NT-based DSC. Noncurling, freestanding, large-area aligned doubly open-ended TiO$_2$ NTs were prepared using a simple selective etching process. The process is described in detail in Fig. S1,† and the properties of the TiO$_2$ NTs have been reported previously.[8] The amorphous freestanding doubly open-ended TiO$_2$ NTs were transferred to the FTO substrate with a 2 μm thick TiO$_2$ NP film (binding layer). The amorphous TiO$_2$ NT film electrode was then annealed at 550 °C for 30 min, which transformed the layer to a crystalline anatase phase (see the XRD data of Fig. S2†). The film was then immersed in a 0.2 M acidic Ti(OH)$_4$ aqueous solution prepared by adding TiCl$_4$ to water and heated at 70 °C for 60 min to induce the formation of TiO$_2$ NPs a few nm in size on the surfaces of the TiO$_2$ NTs. After the decoration step, the electrode was re-annealed to create small anatase TiO$_2$ NPs.

An HR-SEM image of the cross-section of a double-layered NT membrane, detached from the Ti foil, is shown in Fig. 2a. The thin 2nd bottom layer (1 μm) was selectively removed using a simple selective etching process (Fig. 2b) to provide aligned doubly open-ended TiO$_2$ nanotubes (amorphous TiO$_2$ NTs) with
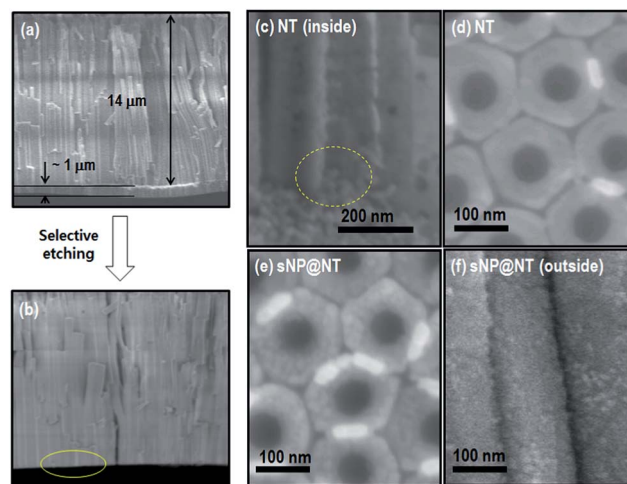

Fig. 2 HR-SEM images: vertical cross-sections of NT arrays detached from the Ti foil (a) before or (b) after removing the bottom layer through a selective etching process. (c) Vertical cross-section of NT arrays transferred to an FTO substrate onto which had been spread a 2 μm thick TiO$_2$ NP layer. (d and e) Top surfaces of the NP and sNP@NT electrodes, respectively. (f) Outside surface of the sNP@NT electrode.

average pore sizes of 110 nm and 60 nm on the top and bottom surfaces (Fig. S3†). The diameter of the top surface exceeded that of the bottom surface; thus, contact between the top surface and the electrode allowed the TiO$_2$ NPs to easily enter the inner tube walls and fill the interfacial gap to provide good electrical connections between the NTs and the NPs (see the dotted line shown in Fig. 2c). The NT surfaces were clearly decorated with TiO$_2$ NPs a few nm in size (sNP@NT) after immersion in a 0.2 M acidic Ti(OH)$_4$ aqueous solution (Fig. 2e), side view shown in Fig. 2f. The raw NTs are shown in Fig. 2d for comparison. Fig. S4† also shows well-decorated inner sides with the small TiO$_2$ NPs. The small TiO$_2$ NPs increased the dye loading and enhanced the electrical contact between the NT arrays and the NPs.

We first optimized the length of the NTs and investigated the effects of the thickness on the photovoltaic performances of DSCs prepared using NT layers with a variety of thicknesses (11–27 μm). The electrodes were sensitized with the dye molecules by immersion in a 0.3 M ethanolic solution of (Bu$_4$N)$_2$Ru(dcbpyH)$_2$(NCS)$_2$ (N719 dye) for 24 h.[23] The TiO$_2$ electrode and semi-transparent Pt-coated FTO (fluorinated tinoxide) counter electrode were sandwiched together using 60 μm thick hot-melt Surlyn spacers. A liquid electrolyte solution composed of 0.03 M I$_2$, 0.6 M 1-butyl-3-methylimidazolium iodide (BMII), 0.1 M guanidinium thiocyanate, 0.5 M LiI and 0.5 M 4-*tert*-butylpyridine in acetonitrile and valeronitrile (85 : 15) was introduced between the sensitized and counter electrodes using a syringe. The photovoltaic parameters of the NT-based DSCs are summarized in Table 1.

Fig. 3a shows the photocurrent–photovoltage (J–V) properties of the NT–DSCs under AM 1.5 solar front illumination. As the length of the NTs increased, the J_{SC} value increased from 13.7 (11 μm) to 17.6 mA cm^{-2} (27 μm). The J_{SC} value did not increase
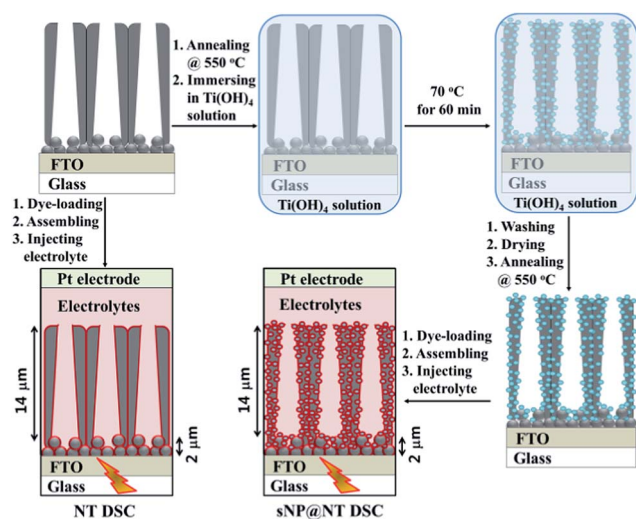

Fig. 1 Schematic illustration of the process used to fabricate an sNP@NT-based DSC.

14382 | *J. Mater. Chem. A*, 2014, **2**, 14380–14385

This journal is © The Royal Society of Chemistry 2014

Table 1 Photocurrent–voltage characteristics of the DSCs fabricated with TiO_2 NT layers with various thicknesses under AM 1.5 irradiation

TiO_2	t^a (μm)	V_{OC} (V)	J_{SC} (mA cm^{-2})	FF (%)	η (%)
NT	6 + 2	0.801 ± 0.021	9.6 ± 0.2	0.625 ± 0.019	4.8 ± 0.2
NT	11 + 2	0.752 ± 0.012	13.7 ± 0.3	0.663 ± 0.007	6.8 ± 0.3
NT	14 + 2	0.710 ± 0.008	16.9 ± 0.3	0.680 ± 0.016	8.2 ± 0.2
NT	20 + 2	0.700 ± 0.007	17.0 ± 0.4	0.660 ± 0.005	7.8 ± 0.2
NT	27 + 2	0.680 ± 0.011	17.6 ± 0.3	0.630 ± 0.020	7.4 ± 0.3

^{a} Thicknesses of the TiO_2 electrodes. NTs were placed on a NP (20 nm in size) layer of 2 μm thick. Cell size: 0.15–0.25 cm^2. Values are reported as the average of the values obtained from 4 devices.
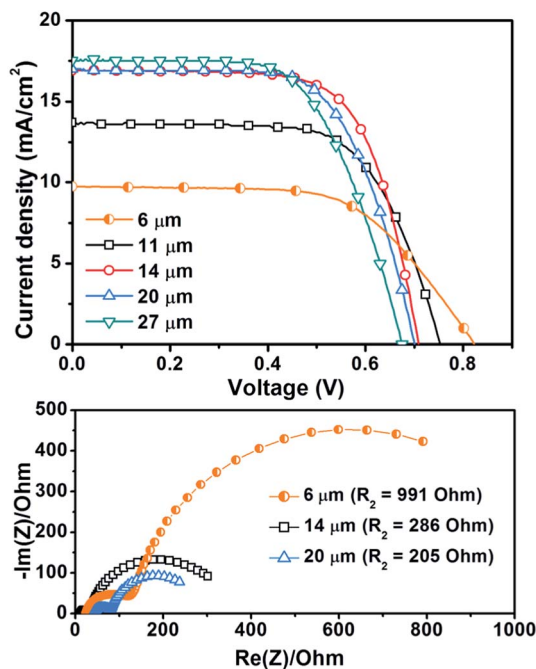

Fig. 3 (a) Representative photocurrent–photovoltage (J–V) properties of the NT-based DSCs prepared with 11–27 μm thick NT layers. (b) Nyquist plots for the NT-based DSCs prepared with 6, 14, and 20 μm thick NT layers, measured at −0.69 V in the dark.

significantly for layer thicknesses beyond 14 μm, which gave a J_{SC} value of 16.9 mA cm^{-2}. The J_{SC} value depended mainly on the quantity of dye adsorbed onto the NT surfaces, which was measured by detaching the dyes from the electrodes in a 0.1 M KOH solution and measuring the solution dye concentration using UV-Vis spectrophotometry (Fig. S5 and S6†).[24,25] As mentioned, J_{SC} was strongly related to η_{inj} ($J_{SC} = q \times \eta_{lh} \times \eta_{inj} \times \eta_{cc} \times I_o$). The value of η_{inj} could be influenced by the energy gap between the energy levels of the lowest unoccupied molecular orbital (LUMO) and the quasi conduction band (CB), as well as by the dye adsorption mode or the presence of aggregation on the TiO_2 electrode surfaces.[24] In this study, the values of η_{inj} did not vary because the NT preparation and dye sensitization steps were performed under identical conditions. Therefore, J_{SC} was expected to be proportional to the light harvesting ability of the dyes and the quantity of dye adsorbed onto the electrodes (η_{lh}).

The increase in J_{SC} was not correlated with the increase in the quantity of dye adsorbed onto the electrodes. The value of η_{cc} strongly influenced the photoinduced electron loss mechanisms caused by recombination of the electrons and I_3^- in the electrolyte.[26]

The highest PCE (8.2%) for a $J_{SC} = 16.9$ mA cm^{-2}, a $V_{OC} = 0.710$ V, and a FF = 0.680 was obtained from a DSC prepared with a 14 μm thick NT layer. Interestingly, the V_{OC} values gradually decreased from 0.752 (11 μm) to 0.680 V (27 μm) as the NT layer thickness increased. This trend was ascribed to the relative drop in J_{SC} in the thicker NT layers, as described by the equation: $V_{OC} = (nkT/q) \times \ln(J_{SC}/J_S)$. Here, n is the device ideality factor, k is the Boltzmann constant, T is the temperature in units of Kelvin, q is the fundamental charge, and J_S is the saturation current density.[27] As the length of the NTs increased, the rate of recombination between photoinduced electrons and I_3^- species or cationic dyes increased, even though the light harvesting properties increased.

We next fabricated sNP@NT-based DSCs using 14 μm thick NT layers (prepared using a 60 min immersion time) to achieve a highly efficient solar cell (Table 2). UV-Vis spectrophotometry measurements revealed that the quantities of N719 dye adsorbed onto the NT electrode were 22% lower than the values obtained from the NP electrodes (Fig. 4a). Meanwhile, the quantity of dye loaded onto the sNP@NT-based DSC was 9% higher than that of the NT electrode, indicating that the TiO_2 sNPs were introduced onto the surface of the doubly open-ended NTs. Fig. 4b shows a comparison between the photocurrent–photovoltage (J–V) properties of the sNP@NT-based DSC and the NT-based DSC. As mentioned above, the PCE of the NT-based DSC was 8.2%, with $J_{SC} = 17.1$ mA cm^{-2}, $V_{OC} = 0.710$ V, and a FF = 0.680. This value was slightly greater than the value (7.3%) obtained from a conventional NP-based DSC prepared with an identical thickness (16 μm) mainly due to a larger V_{OC} value in the NT-based DSC (0.710 V vs. 0.687 V). Considering that the dye loading onto the NT-based DSC was 22% lower than that of the NP-based DSC, the J_{SC} in the NP-based DSC was expected to exceed the value obtained from the NT-based DSC; however, the J_{SC} values obtained from the NP and NT-based DSCs were similar, indicating the presence of a dominant photoinduced electron loss mechanism, which decreased V_{OC} and J_{SC} in the NP-based DSC.

After decorating the surfaces of the doubly open-ended NTs with small NPs, the PCE of the sNP@NT-based DSC improved to 9.2%, with a J_{SC} of 19.6 mA cm^{-2}, a V_{OC} of 0.686 V, and a FF of 0.680. This PCE was 12% greater than that of the NT-based DSC (8.2%). The J_{SC} value increased from 17.1 to 19.6 mA cm^{-2} (a 14% increase). This improvement over the corresponding NT-based DSC arose mainly from the higher degree of dye loading on the NT surface. The V_{OC} of the sNP@NT-based DSCs decreased to 0.686 V compared to the value (0.710 V) obtained from the NT-based DSCs. As discussed above, the photoinduced electron loss mechanism remained dominant in the 14 μm thick NT layer. Therefore, the presence of additional dye molecules adsorbed onto the surfaces of the small NPs did not significantly increase the value of J_{SC}. In turn, the photoinduced

Table 2 Photocurrent–voltage characteristics for the DSCs fabricated from various TiO₂ NTs under AM 1.5 irradiation

TiO₂	t^a (μm)	V_{OC} (V)	J_{SC} (mA cm^{-2})	FF (%)	η (%)
sNP@NTs	14 + 2	0.686 ± 0.008	19.6 ± 0.1	0.680 ± 0.013	9.2 ± 0.2
NPs	16	0.687 ± 0.012	17.0 ± 0.5	0.630 ± 0.021	7.3 ± 0.3
NTs[b]	14 + 2	0.710 ± 0.008	16.9 ± 0.3	0.680 ± 0.016	8.2 ± 0.2

[a] Thickness of the TiO₂ electrodes. NTs were placed on 2 μm thick NP (20 nm) layers. Cell size: 0.15–0.25 cm². [b] See Table 1 for comparison. The values are reported as the average of the values obtained from 4 devices.
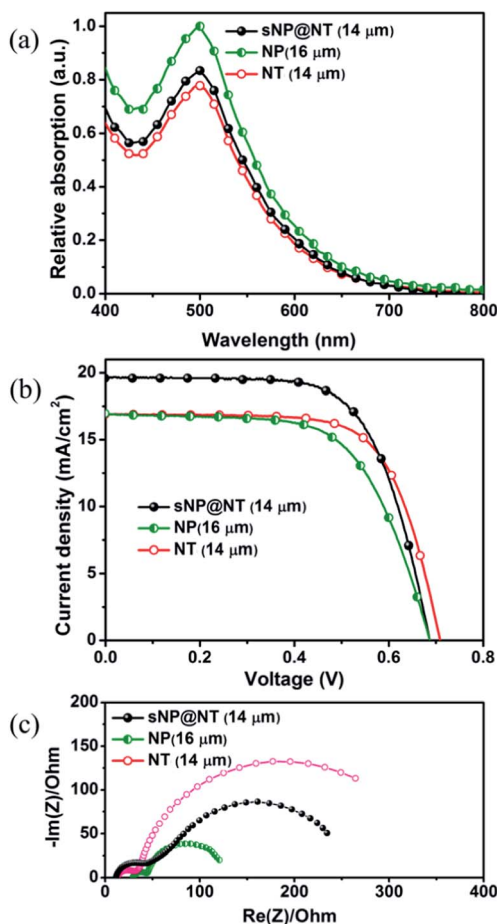

Fig. 4 (a) UV-Vis spectra of the N719 dyes detached from the electrodes in a 0.1 M KOH solution. (b) The photocurrent–photovoltage (J–V) properties of the DSCs fabricated with sNP@NTs, NTs, or NPs. (c) Nyquist plots for the DSCs fabricated with sNP@NTs, NTs, and NPs measured at −0.69 V in the dark.

electron loss mechanism slightly reduced V_{OC} in the sNP@NT-based DSC.

The resistance to recombination (R_{rec}) between sNP@NT and I₃⁻, obtained using EIS measurements at −0.69 V in the dark (Fig. 4c), was 232 Ω, slightly smaller than the value measured between NTs and I₃⁻ (286 Ω); however, both values were much greater than the R_{rec} between NPs and I₃⁻ (84 Ω).

The PCE (9.2%) of the sNP@NT-based DSCs was even greater than the PCE of a conventional NP-based 5 μm thick DSC prepared using a 400 nm thick TiO₂ scattering layer (denoted SL@NP-based DSC) and an active layer with an identical thickness (16 μm), which displayed J_{SC} = 19.1 mA cm^{-2}, V_{OC} = 0.678 V, FF = 0.622, and provided a PCE = 8.1%. It should be noted that this PCE exceeded that obtained from the NP-based DSC (7.3%) due to the scattering effects, consistent with the results reported by others.[28]

We further improved the PCE of the sNP@NT-based DSC by introducing a thinner NT layer (11 μm thickness). The sNP@NT-based DSC (11 μm NT) provided a J_{SC} = 19.8 mA cm^{-2}, with a maximum incident photon-to-current conversion efficiency (IPCE) value of 94.3% (Fig. S7†), a V_{OC} = 0.745 V, and a FF = 0.678, resulting in an estimated PCE of 10.0%. These improvements were mainly ascribed to the larger V_{OC} value compared to the value obtained from the sNP@NT-based DSC (14 μm NT, Fig. 5). Frank et al. reported that the theoretical maximum PCE of the N719-sensitized cell employing the triiodide/iodide redox couple is 14.3% with the values for the fill factor ranging from 0.65 to 0.75 and V_{OC} ranging from 0.7 to 0.8 V, and this value would be achieved with no recombination reactions on the surfaces of TiO₂/dye/electrolyte.[29] As shown in Fig. 4c and our previous report,[8] NT based DSCs show higher recombination resistance and charge collection efficiency than those of NP based DSCs, thus the resulting PCE of NT based DSCs could be more close to the theoretical maximum PCE of DSCs compared with conventional NP based DSCs. It should be noted that more
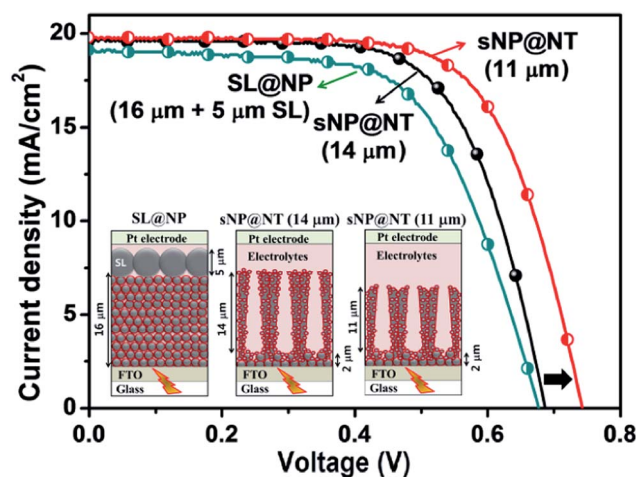

Fig. 5 Comparison of the photocurrent–photovoltage (J–V) properties of three different DSCs: two sNP@NT-based DSCs fabricated with NT array layers of 11 or 14 μm thick, and a conventional DSC prepared with a 16 μm thick active layer composed of 20 nm TiO₂ NPs and a 5 μm thick scattering layer composed of 400 nm TiO₂ NPs.

decoration of the NTs with TiO_2 NPs a few nm in size (80 min *versus* 60 min in sNP@NT) did not effectively improve the PCE (Fig. S8†), most likely due to dominant recombination reaction on the surfaces of the small TiO_2 NPs (Fig. S9†).

4. Conclusions

We demonstrated the preparation of a highly efficient dye-sensitized solar cell using a doubly open-ended TiO_2 NT array decorated with TiO_2 NPs a few nm in size. The small NPs were readily introduced by immersing the NT array in a $Ti(OH)_4$ aqueous solution at 70 °C for 60 min. The front-side illuminated sNP@NT-based DSC exhibited a greatly enhanced PCE of 10.0% (a 47% improvement over the PCE of the NT-based DSCs). This PCE exceeded that of the conventional SL@NP-based DSCs (8.1%). The improved PCE in the sNP@NT arose from both a larger surface area with a higher dye loading (thus, enhanced light-harvesting ability) and a low electron transfer resistance (thus, a slower recombination reaction). This approach is being extended to the preparation of iodine-free solid state DSCs with various sensitizers and hole transporting materials.

Acknowledgements

Notes and references

1 B. O'Regan and M. Grätzel, *Nature*, 1991, **353**, 737–740.
2 S.-H. Park, I. Y. Song, J. Lim, Y. S. Kwon, J. Choi, S. Song, J. R. Lee and T. Park, *Energy Environ. Sci.*, 2013, **6**, 1559–1564.
3 S.-H. Park, J. Lim, I. Y. Song, J.-R. Lee and T. Park, *Adv. Energy Mater.*, 2014, DOI: 10.1002/aenm.201470013.
4 K. Zhu, N. R. Neale, A. Miedaner and A. J. Frank, *Nano Lett.*, 2007, **7**, 69–74.
5 P. Roy, D. Kim, I. Paramasivam and P. Schmuki, *Electrochem. Commun.*, 2009, **11**, 1001–1004.
6 J. H. Seo, A. Gutacker, Y. Sun, H. Wu, F. Huang, Y. Cao, U. Scherf, A. J. Heeger and G. C. Bazan, *J. Am. Chem. Soc.*, 2011, **133**, 8416–8419.
7 E. Ramasamy, W. J. Lee, D. Y. Lee and J. S. Son, *Electrochem. Commun.*, 2008, **10**, 1087–1089.
8 J. Choi, S. Park, Y. Kwon, J. Lim, I. Song and T. Park, *Chem. Commun.*, 2012, **48**, 8748–8750.
9 B.-X. Lei, J.-Y. Liao, R. Zhang, J. Wang, C.-Y. Su and D.-B. Kuang, *J. Phys. Chem. C*, 2010, **114**, 15228–15233.
10 S.-H. Park, J. Lim, Y. S. Kwon, I. Y. Song, J. M. Choi, S. Song and T. Park, *Adv. Energy Mater.*, 2013, **3**, 184–192.
11 J. Park, S. Bauer, K. von der Mark and P. Schmuki, *Nano Lett.*, 2007, **7**, 1686–1691.
12 J. Park, S. Bauer, K. A. Schlegel, F. W. Neukam, K. von der Mark and P. Schmuki, *Small*, 2009, **5**, 666–671.
13 S. E. John, S. K. Mohapatra and M. Misra, *Langmuir*, 2009, **25**, 8240–8247.
14 D. Kim, A. Ghicov, S. P. Albu and P. Schmuki, *J. Am. Chem. Soc.*, 2008, **130**, 16454–16455.
15 S. P. Albu, D. Kim and P. Schmuki, *Angew. Chem., Int. Ed.*, 2008, **47**, 1916–1919.
16 C.-C. Chen, H.-W. Chung, C.-H. Chen, H.-P. Lu, C.-M. Lan, S.-F. Chen, L. Luo, C.-S. Hung and E. W.-G. Diau, *J. Phys. Chem. C*, 2008, **112**, 19151–19157.
17 J. Lin, X. Liu, M. Guo, W. Lu, G. Zhang, L. Zhou, X. Chen and H. Huang, *Nanoscale*, 2012, **4**, 5148–5153.
18 (*a*) Z. Zhang, Z. Yang, Z. Wu, G. Guan, S. Pan, Y. Zhang, H. Li, J. Deng, B. Sun and H. Peng, *Adv. Energy Mater.*, 2014, DOI: 10.1002/aenm.201301750; (*b*) S. Pan, Z. Yang, H. Li, L. Qiu, H. Sun and H. Peng, *J. Am. Chem. Soc.*, 2013, **135**, 10622–10625; (*c*) H. Sun, Z. Yang, X. Chen, L. Qiu, X. You, P. Chen and H. Peng, *Angew. Chem., Int. Ed.*, 2013, **52**, 8276–8280.
19 A. Lamberti, A. Sacco, S. Bianco, D. Manfredi, F. Cappelluti, S. Hernandez, M. Quaglioa and C. F. Pirriab, *Phys. Chem. Chem. Phys.*, 2013, **15**, 2596–2602.
20 S. Kurian, P. Sudhagar, J. Lee, D. Song, W. Choi, S. Lee, Y. S. Kang and H. T. Jeon, *J. Mater. Chem. A*, 2013, **1**, 4370–4375.
21 L.-Y. Lin, C.-Y. Chen, M.-H. Yeh, K.-W. Tsai, C.-P. Lee, R. Vittal, C.-G. Wu and K.-C. Ho, *J. Power Sources*, 2013, **243**, 535–543.
22 C.-J. Lin, W.-Y. Yu and S.-H. Chien, *J. Mater. Chem.*, 2010, **20**, 1073–1077.
23 J. Lim, Y. S. Kwon, S.-H. Park, J. Choi and T. Park, *Langmuir*, 2011, **27**, 14647–14653.
24 J. Lim, Y. Kwon and T. Park, *Chem. Commun.*, 2011, **47**, 4147–4149.
25 S.-H. Park, J. Lim, I. Y. Song, N. Atmakuri, S. Song, Y. S. Kwon, J. M. Choi and T. Park, *Adv. Energy Mater.*, 2012, **2**, 219–224.
26 G. Schlichthorl, N. G. Park and A. J. Frank, *J. Phys. Chem. B*, 1999, **103**, 782–791.
27 S. Y. Huang, G. Schlichthörl, A. J. Nozik, M. Grätzel and A. J. Frank, *J. Phys. Chem. B*, 1997, **101**, 2576–2582.
28 J. R. Jennings, A. Ghicov, L. M. Peter, P. Schmuki and A. B. Walker, *J. Am. Chem. Soc.*, 2008, **130**, 13364–13372.
29 A. J. Frank, N. Kopidakis and J. V. D. Lagemaat, *Coord. Chem. Rev.*, 2004, **248**, 1165–1179.

This journal is © The Royal Society of Chemistry 2014

J. Mater. Chem. A, 2014, **2**, 14380–14385 | **14385**